Chapter 10

Lines

Introduction

Absorption and emission lines in stellar atmospheres arise from bound-bound transions in atoms and molecules. Lines are important for at least the following reasons:

1. Relative lines strengths depend on the state of ionization and excitation of an atmosphere, which largely depends on the temperature. Thus, lines are an important temperature diagnostic. This also explains why spectral class is so closely correlated with temperature.

2. The line profile, or more crudely the line width, depend on the density in the atmosphere. Thus, lines are diagnostics of density and, indirectly, surface gravity and luminosity. This explains why luminosity class, which is determined by the line widths, is also correlated with these properties.

3. The line profile is also modified by gas motions, both thermal motions and bulk motions. This allows the lines to be diagnostics of bulk motions, such as rotation, turbulence, and outflows in winds.

4. Changes in the abundance of an element produce more direct changes in line strengths than in the continuum shape, and so we can use lines to determine the chemical composition. This has applications in studying the chemical evolution of our galaxy and, more recently, other galaxies and in studying understanding late-stages of stellar evolution, in which the products of nuclear burning can be "dredged up" to the atmosphere.

5. As we shall see, lines have a finite width and an opacity that drops away from the line center. Thus, the effect of lines on the opacity is to cause it to vary significantly over a small range in frequency. Lines therefore provide a means to sample a range of depths, from the upper parts of the atmosphere (in the core) to the region of continuum formation (in the far wings). For example, in the Sun, optical depth unity in the visual continuum occurs in the photosphere, but optical depth unity for the optical lines Hα and Ca II H and K occurs in the chromosphere. This is a useful diagnostic tools.

   [*Include a figure like 7-32 of Mihalas.*]

6. The interplay of line opacity and velocity gradients determines the acceleration of the winds in early-type stars.

Macroscopic and Microscopic Processes

We can divide line broadening mechanisms according to whether they are microscopic or macroscopic.

Macroscopic broadening is the result of large-scale motions in the atmosphere, such as rotation, pulsation, and the wind. The relative motion of different parts of the atmosphere causes their line profiles to be shifted according to the Doppler shift. When we average over the atmosphere to obtain a flux, we average over these shifted profiles, and the result is a profile that is broader but shallower.

Microscopic broadening is a local process that changes the line profile over scales much smaller than $\tau = 1$. There are four microscopic broadening processes: natural broadening due to their finite lifetimes of excited state, pressure broadening due to the effects of surrounding particles, thermal broadening due to thermal motion, and microturbulence.

The Line Profile

Natural Broadening

We normally think of excited states as having precise energies. For example, when we learn quantum mechanics we model the hydrogen atom using the time-independent Schrödinger equation and obtain precise energies of the excites states. However, such a treatment is approximate, because an excited hydrogen atom is manifestly not a time-indepenent system – it will eventually decay. When we use the time-dependent Schrödinger equation to model the decay of an excited state to the ground state, we discover that the excited state is a superposition of states having a range of energies. The mean energy is equal to the energy obtained using the time-independent Schrödinger equation, so there are no shifts, but the characteristic width of the distribution in energy is $\hbar/\tau$, in which τ is the mean lifetime of the excited state. This is consistent with the uncertainty principle that $\Delta E \Delta t \sim \hbar$.

One can consider the natural broadening of an emission line as arising from the interplay of the uncertainty principle and the finite lifetime of the upper state. As the upper state has a finite lifetime τ, it no longer can be considered to have a definite energy, but rather must be considered as a superposition of states with a spread in energy of h/τ. If the transition is between two excited states, we must take into account the finite width of both. A detailed quantum mechanical treatment leads to

$$\psi(\nu) = \frac{\Gamma/4\pi^2}{(\nu-\nu_0)^2 + (\Gamma/4\pi)^2}, \tag{10.1}$$

where ν_0 is the central frequency of the line and Γ is the damping width. This is known as the Lorenz profile, and it has a FWHM in frequency of $\Gamma/2\pi$. As shown in Figure 10.1 , at a given FWHM, a Lorenz profile is more sharply peaked and had broader wings than a Gaussian profile.

To calculate Γ, we sum of the individual damping widths of the upper and lower states,

$$\Gamma = \Gamma_u + \Gamma_l. \tag{10.2}$$

The damping width of a state i is given by the reciprocal of the mean lifetime of of the state, which is the sum of the mean lifetimes of all transitions from that state:

$$\Gamma_i = \frac{1}{\tau_i} = \sum_{j\neq i} \frac{1}{\tau_{ij}}. \tag{10.3}$$

The mean lifetime of an excited state of an isolated atom is intimately related to the Einstein coefficients. In a two-level atom, the expressions A_{10}, $B_{10}J_\nu(\nu_{10})$, and $B_{01}J_\nu(\nu_{01})$ give the probability per unit time per atom of spontaneous emission, stimulated emission, and absorption. Thus, the mean lifetime of the upper and lower states are

$$\tau_1 = \frac{1}{A_{10} + B_{10}J_\nu(\nu_{10})} \tag{10.4}$$

and

$$\tau_0 = \frac{1}{B_{01}J_\nu(\nu_{01})}. \tag{10.5}$$

In a multi-level atom, we need to consider all of the transitions that depopulate a state, and so

$$\tau_i = \left[\sum_{j<i} A_{ij} + \sum_{j\neq i} B_{ij}J_\nu(\nu_{ij})\right]^{-1}. \tag{10.6}$$

Pressure Broadening

Pressure broadening is the result of the interaction of the emitting atom with the surrounding particles. It is a slight misnomer because, as we shall see, it leads to both a broadening and a displacement of the central wavelength. Classically there are two components to pressure broadening: impact broadening and statistical broadening.

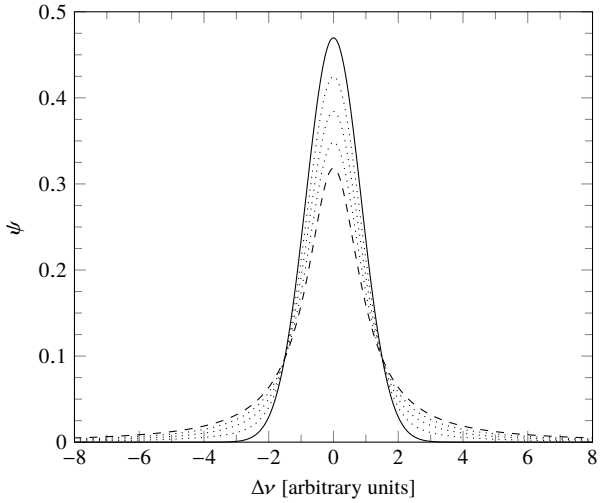

Figure 10.1: Gaussian (solid), Lorentzian (dashed), and Voigt (dotted) line profiles with the same FWHM of 2 in units of $\Delta\nu$.

Classically, one can consider impact broadening to be the result of perturbations by passing particles. These will disturb the emission process and, in effect, introduce phase changes into the emitted wave. The effect of these phase changes is to produce a shifted Lorentz profile; strong encounters dominate the broadening and weak encounters the shift.

Classically, one can consider statistical broadening to be the result of the emitting particle finding itself in a field due to the presense of surrounding particles, which are considered static. Because the positions of the surrounding particles will vary, the field will be slightly different for every emitting particle. This field will effect the energy level structure of the emitting particles, and will lead to a broadening when the emitters are considered as an ensemble. The most important application of this is linear Stark broadening in hydrogenic atoms. The $2n^2$ sublevels of each energy levels in an isolated hydrogenic atoms are degenerate, but split when a field is applied. Further, the splitting is directly proportional to the field strength. Thus, each hydrogenic atom in a plasma will have its energy levels split by a different amount, and this will lead to line broadening. The profile will not in general be a Lorentzian.

Although the classical ideas are useful to understand the effects, quantum mechanical calculations now are used for research purposes. The resulting profiles are similar to but not identical to Lorentzians.

[*Need to give the approximate forms, and state that the shifts and broadning are proportional to the density.*]

Thermal Broadening

If the plasma has a thermal distribution of velocities, the probability density of finding a particle with a line-of-sight velocity ζ

is the Gaussian

$$p(\zeta) = \pi^{-1/2}\zeta_0^{-1}\exp(-\zeta^2/\zeta_0^2), \tag{10.7}$$

where $\zeta_0 \equiv (2kT/m)^{1/2}$ and m is the mass of the particle. The motion will cause the line to be emitted with a frequency of $\nu_0(1+\zeta/c)$ in the observer's frame, and so the emitted profile will be the Gaussian

$$\psi(\nu) = \pi^{-1/2}\Delta\nu_0^{-1}\exp(-\Delta\nu^2/\Delta\nu_0^2), \tag{10.8}$$

where $\Delta\nu \equiv \nu - \nu_0$ and the thermal Doppler width $\Delta\nu_D$ is defined by $\Delta\nu_D \equiv \nu_0\zeta_0/c$. The absorption profile will be identical.

Microturbulence

Lines in real stars are observed to be slightly broader than expected from the combination of natural broadening, pressure broadening, and thermal broadening. This is usually attributed to "microturbulence", or small scale random motions of the gas provoked by convection. We typically assume that the contribution is Gaussian, and so the total Doppler width is given by the micro-turbulent velocity width ζ_{th} added in quadrature with the thermal velocity ζ_0,

$$\zeta_{total}^2 = \zeta_{turb}^2 + \zeta_0^2.$$

For Sun-like stars, values of $\zeta_{turb} \approx 2$ km s^{-1} are typical. The velocities increase with increasing effective temperature and decreasing gravity, for example, ranging from about 1 km s^{-1} for K0V stars to 6 km s^{-1} for F5V stars and from 2 km s^{-1} for G5V stars to 10 km s^{-1} for G5Ib stars.

Total Line Profiles

If we consider the line broadening mechanisms to act independently, we can determine the total line profile by convolving the individual profiles due to each broadening mechanism. Convolving Gaussians is easy: the result is a Gaussian whose FWHM is the quadrature sum of the FWHMs of the individual Gaussians. Perhaps surprisingly, convolving Lorentzians is equally simple: the result is a Lorentzian whose FWHM is the sum of the FWHM of the individual Lorenzians. However, when we convolve a Lorentizan and a Gaussian, we obtain a Voigt profile $H(a,v)$ which is given by

$$\phi(\nu) = H(a,x) = \frac{a}{\pi}\int_{-\infty}^{+\infty}\frac{e^{-y^2}}{(x-y)^2+a^2}\,dy, \tag{10.9}$$

where $x \equiv (\nu-\nu_0)/\Delta\nu_D$ and $a \equiv \Gamma/4\pi\Delta\nu_D$. (In deriving this, we have assumed that $\zeta_0 \ll c$, which is appropriate for stellar atmospheres.) Unfortunately, there is no closed form of the integral: it has to be evaluated numerically (or approximated).

Figure 10.1 shows pure Gaussian and pure Lorentzian profiles as well as several intermediate Voigt profiles. All of these profiles have the same FWHM and same normalization. We can see that the effect of increasing the contribution of the Lorentzian is to lower the core and raise the wings of the the profile.

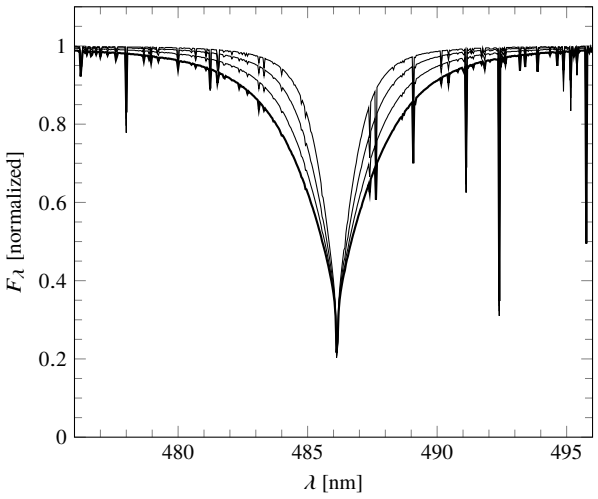

Figure 10.2: Emergent normalized fluxes in the region of Hβ for ATLAS12 model atmospheres for $\log g$ = 3.5, 4.0, 4.5, and 5.0 (thick) and T_{eff} = 10000 K. Note that the line becomes narrower as the surface gravity decreases.

Table 10.1: Strömgren-Crawford Diagnostics in BAFG Stars

Parameter	BA	FG
T_{eff}	$b-y$ or c_1	$b-y$
$\log g$	Hβ	c_1
Z		m_1

[*Compare FWHM of the three components for say* Hβ *in the Sun.*]

Line Width as a Gravity Diagnostic

The density increases with surface gravity at a given effective temperature. As the density increases, pressure broadening becomes more important and the observed widths of strong lines such as Hβ increase. This is shown in Figure 10.2. Thus, supergiants have narrower lines than giants, and giants have narrower lines than dwarfs.

The line profile can be measured spectroscopically, of course, but Crawford (1958) developed a more efficient means to measure its apparent width using filters. He defined two filters centered roughly on the strong Hβ line, one narrow filter β_n with a FWHM of about 3 nm, and one wider filter β_w with a FWHM of about 15 nm. Their profiles are shown in Figure 10.3. The narrow filter essentially measures the depth of the line in the core and the wider filter essentially measures the surrounding continuum. The ratio of the two, in the form of the Hβ index, gives an estimate of the relative depth of the line. Figure 10.4 gives a theoretical calibration.

Crawford photometry is used to complement Strömgren pho-

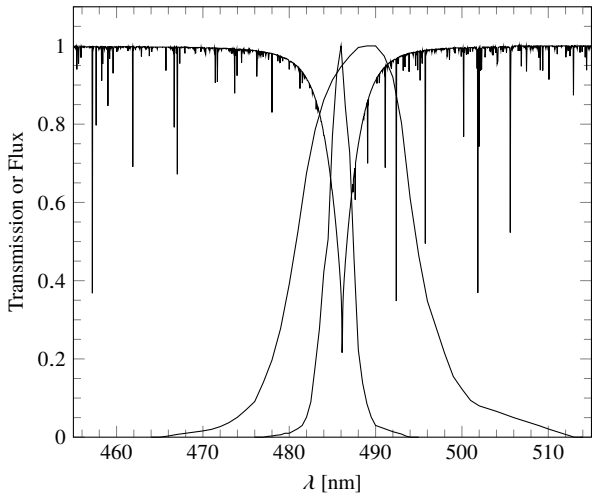

Figure 10.3: The Crawford β_n narrow and β_w wide filters compared to a stellar spectrum. The filter transmissions are from Crawford & Mander (1966) as tabulated by Castelli & Kurucz (2006).

tometry. We have seen that Strömgren photometry of FG stars can be used to measure $T_{\rm eff}$ (from the $b-y$ color) and $\log g$ (from the c_1 index). Strömgren-Crawford photometry for BA stars can be used to measure $T_{\rm eff}$ (from $b-y$ color and c_1 index) and $\log g$ (from the Hβ index). These diagnostics are summarized in Table 10.1.

Equivalent Width

We can define a hypothetical "continuum flux" F_ν^c at the frequency of a line as the flux we would observe if the line had no opacity but otherwise the atmosphere was unchanged. (This is not self consistent; removing a line will change the temperature structure of an atmosphere.) Often we will approximate this by simply interpolating the flux from the continuum on either side of the line.

We can then define the normalized absorption depth A by

$$A \equiv 1 - (F_\nu/F_\nu^c), \tag{10.10}$$

and also the normalized residual flux R by

$$R \equiv (F_\nu/F_\nu^c) = 1 - A. \tag{10.11}$$

These are obviously just the fraction of the continuum flux removed by the line and remaining. In the Sun, we can define these in terms of the specific intensity as functions of μ.

As we observe a the spectrum of a star at higher resolution, each pixel in our detector detectos fewer photons (if the spectrograph efficiency remains constant), and so the spectrum becomes noisier. Thus, we often cannot observe at a sufficiently high resolution to determine the profile of a line, but instead must measure

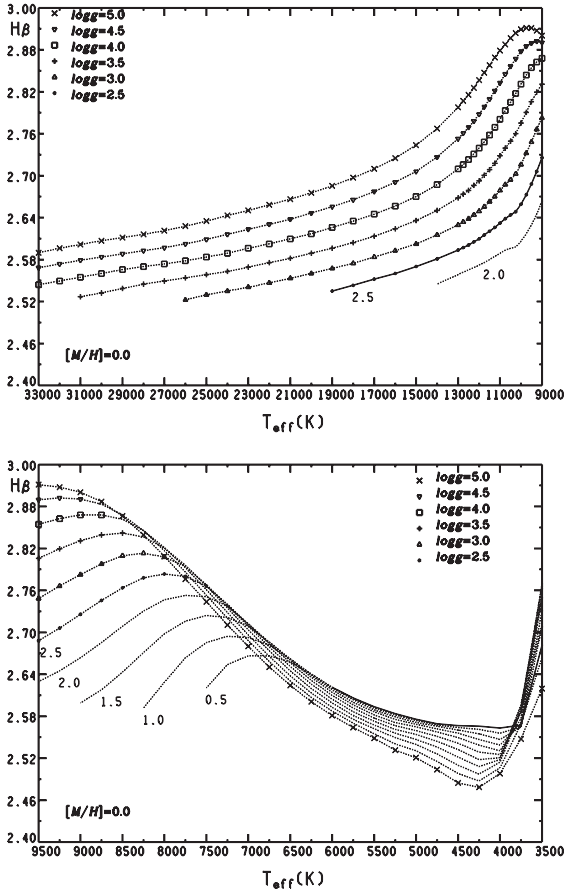

Figure 10.4: The Crawford Hβ index for solar-metallicity stars as predicted from ATLAS9 LTE model by Castelli & Kurucz (2006). For BA stars, with $T_{\rm eff}$ from 7500 to 20,000 K, the Hβ index is an excellent indicator of surface gravity.

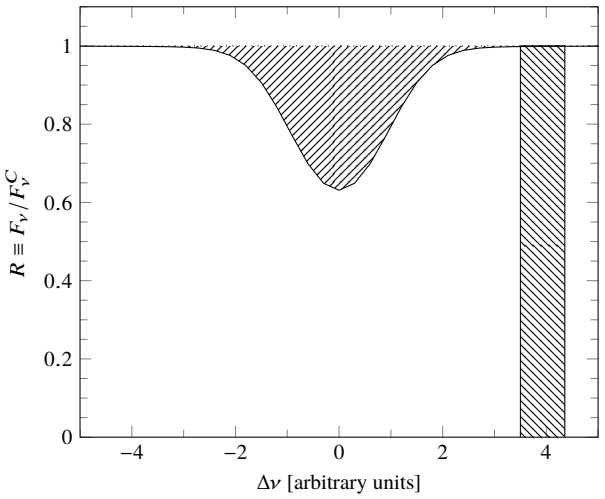

Figure 10.5: An example of the equivalent width. The area between normalized residual flux $R \equiv F_\nu / F_\nu^C$ (solid line) and the normalized continuum (dotted line) is about 0.86 in these arbitrary frequency units. Thus, the equivalent width of the line is 0.86. This is also the area of the rectangle, which has a width of 0.86.

the equivalent width W defined by

$$W = \int_0^\infty A \, d\nu, \tag{10.12}$$

or, much more commonly,

$$W = \int_0^\infty A \, d\lambda. \tag{10.13}$$

The equivalent width is an integrated quantity, and corresponds to the width in frequency or wavelength of an imaginary rectangular line that is completely opaque and has the same "area" as the real line. This shown in Figure 10.5.

One of the most useful properties of the equivalent width is that it is independent of the spectrograph resolution. This is because the finite resolution of a spectrograph effectively acts to convolve the spectrum with a response function. A little consideration shows that this convolution broadens the line, but keeps its total area relative to the continuum constant. However, this constant quantity is exactly the equivalent width.

The Curve of Growth

The curve of growth is a plot of the equivalent width W of an absorption line against the product of the column density in an absorber N and the oscillator strength f. The product Nf is a measure of how strong a line is, and ploting this product allows different lines to be plotted on the same graph by normalizing all of the lines by this notional strength.

The curve of growth is an important tool for understanding the behaviour of spectral lines. Historically, it was very important in abundance measurements, both in stellar atmospheres and ther ISM, but now it has been largely replaced by more direct modelling of stellar atmospheres and ISM absorption profiles.

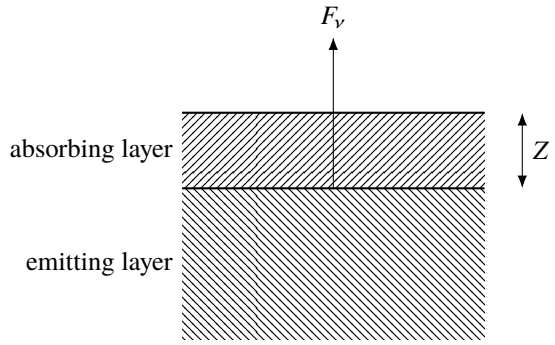

Figure 10.6: The geometry of the simple model for the curve of growth. An absorbing layer of thickness Z and density n lies above an emitting layer. We consider only upward rays.

Let's consider a simple model of a uniform line absorbing layer overlying a continuum emitting layer, as shown in Figure 10.6. This is not a realistic model of an atmosphere – an atmosphere is not uniform and the emitting and absorbing layers are intermixed – but it is a useful first approximation. Furthermore, we will assume that the emitted continuum intensity F_ν^C is sharply peaked in the outward direction (which allows us to ignore an integration over solid angle). This allows us to write the emergent flux as

$$F_\nu = F_\nu^C e^{-\tau}, \tag{10.14}$$

where τ is the normal optical depth though the line absorbing layer. The equivalent width is given by

$$W = \int_0^\infty d\nu A_\nu \tag{10.15}$$

$$= \int_0^\infty d\nu \left(1 - \frac{F_\nu}{F_\nu^C}\right) \tag{10.16}$$

$$= \int_0^\infty d\nu \, (1 - e^{-\tau}) \, . \tag{10.17}$$

The optical depth is given by

$$\tau(\nu) = \int dz \, \alpha(\nu) \tag{10.18}$$

$$= \alpha(\nu) Z \tag{10.19}$$

$$= \left(\frac{\pi e^2}{m_e c}\right) nZ f \phi(\nu) \tag{10.20}$$

$$= \left(\frac{\pi e^2}{m_e c}\right) N f \phi(\nu) \tag{10.21}$$

$$= T \phi(\nu) \tag{10.22}$$

in which the column density N is given by

$$N \equiv nZ \tag{10.23}$$

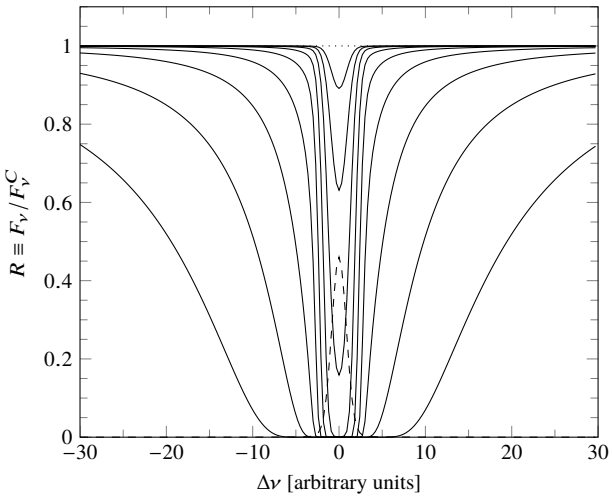

Figure 10.7: The observed residual flux $R \equiv F_\nu / F_\nu^C$ for the simple model for the curve of growth. The dashed line is the assumed line profile. The dotted line is the continuum. The solid lines are the emergent fluxes F_ν for total line opacity $T = \int d\nu\, \tau$ of 1/4, 1, 4, 16, . . . , 16384.

and the optical depth integrated over the line T is given by

$$T \equiv \int d\nu\, \tau(\nu) \tag{10.24}$$

$$= \left(\frac{\pi e^2}{m_e c}\right) N f. \tag{10.25}$$

Thus, we see that in general the equivalent width depends both on the line strength (Nf or T) and on the line profile (ϕ).

We now consider three cases, of increasing line strength.

(a) Weak lines.

For weak lines, $\tau \ll 1$ and so we can approximate $e^{-\tau}$ as $1 - \tau$. In this case, we have

$$W = \int d\nu \tau(\nu) \tag{10.26}$$

$$= T \int_0^\infty d\nu' \phi(\nu') \tag{10.27}$$

$$= T \tag{10.28}$$

Thus, we have $W = T$ the curve of growth will be linear.

(b) Lines saturated in the Gaussian core.

Eventually, the line will *saturate* when the optical depth in the line center is large and the residual flux in this part of the line falls essentially to zero. This can be seen in Figure 10.7. In this case, the contribution of the central part of the line to W will cease to grow and W grows only as the central part widens. The transition from the optically thick core the the optically thin wings will be abrupt, and the absorption line profile becomes quite rectangular. In Figure 10.7, this regime corresponds to $T = 16$ to $T = 256$

The equivalent width will be roughly the FW at the point that the optical depth in the line reaches 1. Thus,

$$1 \approx T\phi(\nu_0 + W/2) \tag{10.29}$$

Since the core is a Doppler profile, we have

$$1 \approx T\pi^{-1/2}\Delta\nu_0^{-1} \exp(-W^2/4\Delta\nu_0^2) \tag{10.30}$$

or

$$\exp(W^2/4\Delta\nu_0^2) \approx T\pi^{-1/2}\Delta\nu_0^{-1} \tag{10.31}$$

or

$$W \propto 2\Delta\nu_0 \left[\ln(T\pi^{-1/2}\Delta\nu_0^{-1})\right]^{1/2}. \tag{10.32}$$

This is known as the flat or saturated part of the curve of growth, as it grows so slowly – as the square root of the logarithm of the line strength. In Figure 10.7, it corresponds to the crowding of lines from about $T = 16$ to $T = 256$, in which even though the total opacity of the line increases by a factor of 16, the area corresponding to the equivalent width only grows moderately.

(c) Lines saturated in the Lorentzian wings.

Eventually, though, the Lorentzian damping wings become important. Again, approximating the line as a rectangle (although this is now no longer such a good approximation), we have

$$1 \approx T \frac{\Gamma/4\pi^2}{(W/2)^2 + (\Gamma/4\pi)^2}, \tag{10.33}$$

but when $W \gg \Gamma$,

$$1 \approx T \frac{\Gamma/4\pi^2}{(W/2)^2}, \tag{10.34}$$

or

$$W \approx \pi^{-1}\sqrt{T\Gamma} \tag{10.35}$$

This is known as the square-root or damped part of the curve. Growth resumes as $\sqrt{T}$, which is faster than in the flat part but not as fast as in the linear part. In Figure 10.7, it corresponds to the crowding of lines above $T = 256$, in which the area starts to grow again more rapidly than in the saturated regime.

Figure 10.8 shows the theoretical curve of growth for the profile in Figure 10.7. The linear part is below $\log T \approx 0.5$, the flat part from $\log T \approx 1$ to $\log T \approx 2$, and the square-root part is above $\log T \approx 3$.

The form of the curve of growth is important in the practice of determining abundances from absorption lines. Essentially, the

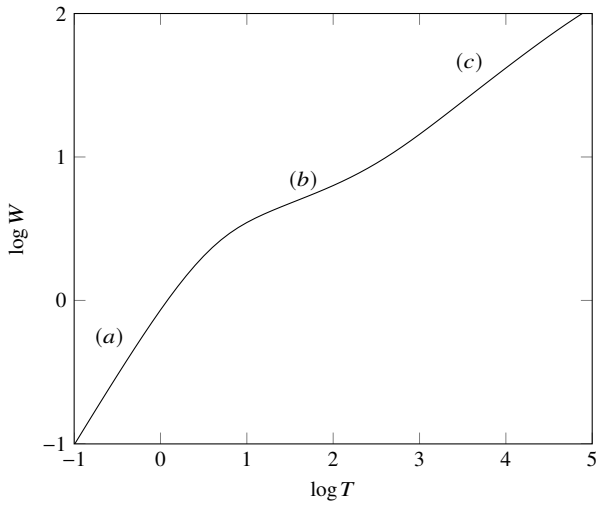

Figure 10.8: The curve of growth for the profile in Figure 10.7. The linear, flat, and square-root regimes are marked by (a), (b), and (c).

idea is that we can measure W and use the curve of growth to determine T with in term gives is the columns density N. If we do this for lines of different species, we can measure their relative abundances.

However, let us for a moment consider that we will always measure W with some uncertainty σ_W. How does this translate into errors in T and hence N? From propagation of uncertainties, we know

$$\sigma_T^2 = \left(\frac{\partial T}{\partial W}\right)^2 \sigma_W^2. \tag{10.36}$$

Since W is monotonic in T, we can simplify this to

$$\sigma_T = \left(\frac{\partial T}{\partial W}\right) \sigma_W. \tag{10.37}$$

Next, we can rearrange this equation to give us the relative uncertainties, σ_W/W and σ_T/T, obtaining

$$T\left(\frac{\sigma_T}{T}\right) = W\left(\frac{\partial T}{\partial W}\right)\left(\frac{\sigma_W}{W}\right) \tag{10.38}$$

$$\left(\frac{\sigma_T}{T}\right) = \left(\frac{W\partial T}{T\partial W}\right)\left(\frac{\sigma_W}{W}\right) \tag{10.39}$$

$$\left(\frac{\sigma_T}{T}\right) = \left(\frac{\partial \ln T}{\partial \ln W}\right)\left(\frac{\sigma_W}{W}\right) \tag{10.40}$$

Thus, for a given fixed uncertainty in the measurement σ_W/W, the uncertainty in the total optical depth and the abundance is larger by a factor of the logarithmic derivative $\partial \ln T/\partial \ln W$. This is the inverse gradient in the curve of growth. In the linear regime this factor is 1; in the flat regime this factor is very much greater than 1; and in the square-root regime this factor is 2. Thus, to obtain the smallest relative errors in the abundance, we should favor first lines in the linear regime, then lines in the square-root regime, and probably not even both with lines in the flat regime.

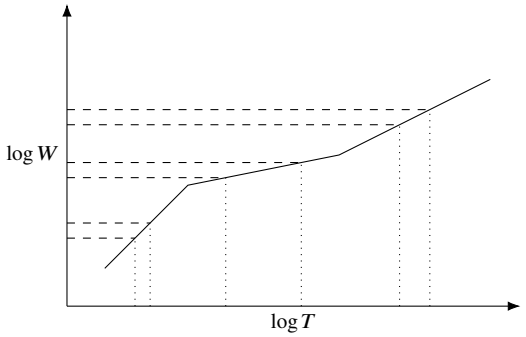

Figure 10.9: Propagation of errors in a schematic curve of growth. For a given relative error in W (represented by the pairs of dashed lines), the relative error in T (represented by the pairs of dotted lines) is smallest in the linear regime, and then next smallest in the square-root regime, and largest by far in the flat regime.

This result can be seen graphically. Consider Figure 10.9, which shows a segment of a hypothetical curve of growth. We represent three measurements of W each with the same relative error as three pairs of dashed lines. These pairs of lines have the same separations, since the axes are logarithmic. We then obtain the corresponding measurements of T by extending dashed lines from the $\log W$ axis to the curve of growth and then extending dotted lines down to the $\log T$ axis. We see that the relative error in T is smallest in the linear regime, then twice as large in the square-root regime, and much larger in the flat regime.

While the curve of growth was used in early studies of abundances, modern studies fit model fluxes from model stellar atmospheres to observed fluxes, iterating and adjusting the abundances in the atmosphere until the best match is found. Nevertheless, the curve of growth tells us while lines will be most sensitive for determining the abundances: weak unsaturated lines and strong damped lines.